

A kinetic model for a polyatomic gas with temperature-dependent specific heats and its application

Kazuo Aoki¹, Shingo Kosuge², and Hung-Wen Kuo¹

¹Department of Mathematics, National Cheng Kung University,
Tainan 70101, Taiwan

²Institute for Liberal Arts and Sciences, Kyoto University,
Kyoto 606-8501, Japan

1 Introduction

In recent years, the study of nonequilibrium polyatomic gas flows based on kinetic theory becomes increasingly important in various applications, such as gas flows in high-temperature circumstances. However, the original Boltzmann equation for a polyatomic gas is usually presented in rather abstract forms because of a lack of knowledge about intermolecular interactions. Therefore, it is impossible to apply it to practical problems immediately. To bypass this difficulty, some simplified and tractable models of the Boltzmann equation have been proposed. One of such models is the ellipsoidal statistical (ES) model proposed by Andries *et al.* [2] and rederived in a systematic way by Brull and Schneider [3].

In a previous paper by two of the present authors [4], this ES model was successfully applied to analyzing the structure of a plane shock wave in a polyatomic gas with large bulk viscosity. However, the ES model in [2] is for a polyatomic gas with constant specific heats (calorically perfect gas). In reality, for most of gases, the specific heats depend on the temperature even if they can be well approximated by ideal gases. The effect of the temperature dependence of the specific heats becomes important when the temperature variation in the gas is large, such as gas flows containing strong shock waves.

For the reason described above, we have extended the ES model in [2] to the case of a polyatomic gas with temperature-dependent specific heats (thermally perfect gas) in our recent paper [5]. In the same reference, the new model equation was also applied to investigating the structure of a plane shock wave with special interest in CO₂ gas, which is known to have a very large bulk viscosity. The numerical and asymptotic analyses there were performed in parallel to the previous paper [4] where a calorically perfect gas is considered. The present paper is intended to provide a summary of [5], so that only the results will be shown, and the details of the proofs and derivations will be omitted.

2 Model Equation

Let us consider a polyatomic rarefied gas. Let t be the time variable, \mathbf{X} (or X_i) the position vector in the physical space, $\boldsymbol{\xi}$ (or ξ_i) the molecular velocity, and \mathcal{E} the energy

associated with the internal modes per unit mass. We denote the total mass of the gas molecules contained in an infinitesimal volume $d\mathbf{X}d\boldsymbol{\xi}d\mathcal{E}$ around a point $(\mathbf{X}, \boldsymbol{\xi}, \mathcal{E})$ in the seven-dimensional space consisting of \mathbf{X} , $\boldsymbol{\xi}$, and \mathcal{E} at time t by

$$f(t, \mathbf{X}, \boldsymbol{\xi}, \mathcal{E})d\mathbf{X}d\boldsymbol{\xi}d\mathcal{E}. \quad (1)$$

The ES model is the equation governing this $f(t, \mathbf{X}, \boldsymbol{\xi}, \mathcal{E})$. In the present study, we consider the thermally perfect gas, for which the specific heat at constant volume C_v and that at constant pressure C_p are both functions of the temperature T and propose a model Boltzmann equation for such a gas, which is a straightforward extension of the ES model for a gas with constant C_v and C_p [2].

We first consider the equilibrium state and assume that the internal energy of the gas per unit mass E is a given (monotonically increasing) function of the temperature T , i.e., $E = E(T)$. We also define a function $D(T)$ as $D(T) = 2E(T)/RT - 3$, where R is the gas constant per unit mass. Note that the relations $C_v(T) = dE(T)/dT$ and $C_p(T) = C_v(T) + R$ hold. Then, we extend $E(T)$, $D(T)$, $C_v(T)$, and $C_p(T)$ in the nonequilibrium case and use them in the definition of the new model equation, which is described as follows.

$$\frac{\partial f}{\partial t} + \xi_i \frac{\partial f}{\partial X_i} = Q(f), \quad (2)$$

with

$$Q(f) = A_c(T)\rho(\mathcal{G} - f). \quad (3)$$

Here,

$$\mathcal{G} = \frac{\rho \mathcal{E}^{\delta/2-1}}{(2\pi)^{3/2} [\det(\mathbb{T})]^{1/2} (RT_{\text{rel}})^{\delta/2} \Gamma(\delta/2)} \times \exp\left(-\frac{1}{2}(\mathbb{T}^{-1})_{ij}(\xi_i - v_i)(\xi_j - v_j) - \frac{\mathcal{E}}{RT_{\text{rel}}}\right), \quad (4a)$$

$$(\mathbb{T})_{ij} = (1 - \theta)[(1 - \nu)RT_{\text{tr}}\delta_{ij} + \nu p_{ij}/\rho] + \theta RT\delta_{ij}, \quad (4b)$$

$$\rho = \iint_0^\infty f d\mathcal{E} d\boldsymbol{\xi}, \quad v_i = \frac{1}{\rho} \iint_0^\infty \xi_i f d\mathcal{E} d\boldsymbol{\xi}, \quad (4c)$$

$$p_{ij} = \iint_0^\infty (\xi_i - v_i)(\xi_j - v_j) f d\mathcal{E} d\boldsymbol{\xi}, \quad (4d)$$

$$T = E^{-1}(e), \quad \delta = D(T) = 2e/RT - 3, \quad (4e)$$

$$T_{\text{tr}} = 2e_{\text{tr}}/3R, \quad T_{\text{int}} = 2e_{\text{int}}/R\delta, \quad T_{\text{rel}} = \theta T + (1 - \theta)T_{\text{int}}, \quad (4f)$$

where e , e_{tr} , and e_{int} are defined by

$$e = e_{\text{tr}} + e_{\text{int}}, \quad e_{\text{tr}} = \frac{1}{2\rho} \iint_0^\infty |\boldsymbol{\xi} - \mathbf{v}|^2 f d\mathcal{E} d\boldsymbol{\xi}, \quad e_{\text{int}} = \frac{1}{\rho} \iint_0^\infty \mathcal{E} f d\mathcal{E} d\boldsymbol{\xi}. \quad (5)$$

In (2)–(5), ρ is the density, \mathbf{v} (or v_i) is the flow velocity, p_{ij} is the stress tensor, e is the internal energy per unit mass, e_{tr} is that associated with the translational motion, e_{int} is that associated with the internal modes, T is the temperature, T_{tr} is the temperature associated with the translational motion, T_{int} is the temperature associated with the energy of the internal modes, $d\boldsymbol{\xi} = d\xi_1 d\xi_2 d\xi_3$, and the domain of integration with respect to $\boldsymbol{\xi}$ is the whole space of $\boldsymbol{\xi}$. The symbol δ_{ij} indicates the Kronecker delta, and $\nu \in [-1/2, 1)$ and $\theta \in [0, 1]$ are parameters. In addition, $A_c(T)$ is a function of T such that $A_c(T)\rho$ is the collision frequency of the gas molecules, $\Gamma(z)$ is the gamma function, \mathbf{T} is the 3×3 positive-definite symmetric matrix whose (i, j) component is defined by (4b), and $\det(\mathbf{T})$ and \mathbf{T}^{-1} are, respectively, its determinant and inverse.

Note that all the macroscopic quantities contained in \mathcal{G} are generated from f . To be more specific, (i) ρ , \mathbf{v} , p_{ij} , e_{tr} , e_{int} , and e are obtained by (4c), (4d), and (5); (ii) T and then δ are determined by (4e) using the inverse function E^{-1} of the function E ; (iii) T_{tr} , T_{int} , and T_{rel} are determined by (4f), and then \mathbf{T} is established by (4b). Since $e = e_{\text{tr}} + e_{\text{int}} = (3T_{\text{tr}} + \delta T_{\text{int}})R/2$ and also $e = (3 + \delta)RT/2$, we have the relation $T = (3T_{\text{tr}} + \delta T_{\text{int}})/(3 + \delta)$ [note that δ depends on T : cf. (4e)].

The pressure p and the heat-flow vector q_i are given by

$$p = R\rho T, \quad (6a)$$

$$q_i = \iint_0^\infty (\xi_i - v_i) \left(\frac{1}{2} |\boldsymbol{\xi} - \mathbf{v}|^2 + \mathcal{E} \right) f d\mathcal{E} d\boldsymbol{\xi}, \quad (6b)$$

where (6a) is the equation of state.

3 Basic Properties

In the following, we summarize the basic properties that follow from the model equation (2). Some properties are different when the parameter θ is equal to zero.

Proposition 1 (conservation for $\theta \neq 0$): For an arbitrary function $f(t, \mathbf{X}, \boldsymbol{\xi}, \mathcal{E})$, the following relation holds:

$$\iint_0^\infty \varphi_r Q(f) d\mathcal{E} d\boldsymbol{\xi} = 0, \quad (7)$$

where φ_r ($r = 0, \dots, 4$) are the collision invariants, i.e.,

$$\varphi_0 = 1, \quad \varphi_i = \xi_i \quad (i = 1, 2, 3), \quad \varphi_4 = \frac{1}{2} |\boldsymbol{\xi}|^2 + \mathcal{E}. \quad (8)$$

Proposition 1' (conservation for $\theta = 0$): For an arbitrary function $f(t, \mathbf{X}, \boldsymbol{\xi}, \mathcal{E})$, the following relation holds:

$$\iint_0^\infty \varphi_r Q(f) d\mathcal{E} d\boldsymbol{\xi} = 0, \quad (9)$$

where φ_r ($r = 0, \dots, 5$) are the collision invariants, i.e.,

$$\varphi_0 = 1, \quad \varphi_i = \xi_i \quad (i = 1, 2, 3), \quad \varphi_4 = \frac{1}{2}|\boldsymbol{\xi}|^2, \quad \varphi_5 = \mathcal{E}. \quad (10)$$

Proposition 2 (equilibrium $\theta \neq 0$): The vanishing of the collision term $Q(f) = 0$ is equivalent to the fact that f is the following local equilibrium distribution:

$$f_{\text{eq}} = \frac{\bar{\rho}\mathcal{E}^{\bar{\delta}/2-1}}{(2\pi R\bar{T})^{3/2}(R\bar{T})^{\bar{\delta}/2}\Gamma(\bar{\delta}/2)} \exp\left(-\frac{|\boldsymbol{\xi} - \bar{\mathbf{v}}|^2}{2R\bar{T}} - \frac{\mathcal{E}}{R\bar{T}}\right), \quad (11)$$

where $\bar{\rho}$, $\bar{\mathbf{v}}$, and \bar{T} are arbitrary functions of t and \mathbf{X} , and $\bar{\delta} = D(\bar{T})$.

Proposition 2' (equilibrium for $\theta = 0$): The vanishing of the collision term $Q(f) = 0$ is equivalent to the fact that f is the following local equilibrium distribution:

$$f_{\text{eq}} = \frac{\bar{\rho}\mathcal{E}^{\bar{\delta}/2-1}}{(2\pi R\bar{T}_{\text{tr}})^{3/2}(R\bar{T}_{\text{int}})^{\bar{\delta}/2}\Gamma(\bar{\delta}/2)} \exp\left(-\frac{|\boldsymbol{\xi} - \bar{\mathbf{v}}|^2}{2R\bar{T}_{\text{tr}}} - \frac{\mathcal{E}}{R\bar{T}_{\text{int}}}\right), \quad (12)$$

where $\bar{\rho}$, $\bar{\mathbf{v}}$, \bar{T}_{tr} , and \bar{T}_{int} are arbitrary functions of t and \mathbf{X} , and $\bar{\delta}$ and \bar{T} are determined by the following coupled equations:

$$\bar{\delta} = D(\bar{T}), \quad \bar{T} = E^{-1}(3R\bar{T}_{\text{tr}}/2 + \bar{\delta}R\bar{T}_{\text{int}}/2). \quad (13)$$

The solution $(\bar{\delta}, \bar{T})$ of (13) exists. In particular, it is unique when $\bar{T}_{\text{int}} \leq \bar{T}_{\text{tr}}$.

Proposition 3: For an arbitrary function $f(t, \mathbf{X}, \boldsymbol{\xi}, \mathcal{E})$, the following inequality holds:

$$\iint_0^\infty \left(\ln \frac{f}{\mathcal{E}^{\delta/2-1}}\right) Q(f) d\mathcal{E} d\boldsymbol{\xi} \leq 0, \quad (14)$$

and the equality sign holds if and only if $f = f_{\text{eq}}$ in (11) ($\theta \neq 0$) or (12) ($\theta = 0$).

Proposition 4 (H theorem for spatially homogeneous case): Let $H_\delta(f)$ be defined by

$$H_\delta(f) = \iint_0^\infty f \ln \frac{f}{\mathcal{E}^{\delta/2-1}} d\mathcal{E} d\boldsymbol{\xi}. \quad (15)$$

If f does not depend on \mathbf{X} , the following inequality holds:

$$dH_\delta/dt \leq 0, \quad (16)$$

and the equality sign holds if and only if $f = f_{\text{eq}}$ in (11) ($\theta \neq 0$) or (12) ($\theta = 0$).

On the basis of the model equation (2) with $\theta \neq 0$, one can carry out the Chapman–Enskog expansion to derive the compressible Navier–Stokes equations and the explicit expressions of the transport coefficients. The latter coefficients are summarized as follows:

Proposition 5 (Transport coefficients for $\theta \neq 0$): Let μ , μ_b , and λ be the viscosity, bulk-viscosity, and thermal-conductivity coefficients, respectively, and let γ and Pr be the ratio of specific heats and the Prandtl number, defined respectively by $\gamma = C_p/C_v = (C_v + R)/C_v$ and $\text{Pr} = C_p\mu/\lambda$. Then, μ , μ_b , λ , and Pr are expressed as follows:

$$\begin{aligned} \mu(T) &= \text{Pr} \frac{RT}{A_c(T)}, & \mu_b(T) &= \frac{1}{\theta} \left[\frac{5}{3} - \gamma(T) \right] \frac{\mu(T)}{\text{Pr}}, \\ \lambda(T) &= \frac{\gamma(T)R}{\gamma(T) - 1} \frac{RT}{A_c(T)}, & \text{Pr} &= \frac{1}{1 - \nu + \theta\nu}, \end{aligned} \quad (17)$$

where the fact that μ , μ_b , λ , and γ depend on the temperature is explicitly shown.

4 Application to Shock-Wave Structure

In this section, we apply the model equation proposed in Sect. 2 to the problem of shock-wave structure. The shock wave is a compression wave across which the physical quantities undergo rapid changes over a distance of some tens of the mean free path. Therefore, to describe the structure inside the shock wave, one has to use kinetic theory or the Boltzmann equation. In fact, the structure of a standing plane shock wave is one of the most fundamental problems in kinetic theory and has been investigated by many authors.

Motivated by some recent and interesting results based on extended thermodynamics [8, 10], we investigated the structure of a plane shock wave in carbon dioxide (CO_2) gas, which is known to have very large bulk viscosity, numerically using the ES model for a gas with constant specific heats (calorically perfect gas) [4]. In [4], some comparisons were made between the result based on the ES model and that based on extended thermodynamics [8], and good agreement was shown. However, the comparisons were restricted to rather weak shock waves in which the temperature variation is not large. The reason is that [8, 10] used the data for CO_2 gas with temperature-dependent specific heats, whereas [4] used the ES model with constant specific heats. For a strong shock wave, the effect of temperature-dependent specific heats becomes more important because of the large temperature variation across the shock. In order to understand this effect, we try to carry out the numerical analysis of the shock profile, with special interest in stronger shock waves, using the model for a gas with temperature-dependent specific heats (thermally perfect) proposed in Sect. 2.

4.1 Problem

Let us consider a stationary plane shock wave standing in a flow of an ideal polyatomic gas. We take the X_1 axis perpendicular to the shock wave. The gas at upstream infinity ($X_1 \rightarrow -\infty$) is in an equilibrium state with density ρ_- , flow velocity $\mathbf{v}_- = (v_-, 0, 0)$ ($v_- > 0$), and temperature T_- , and that at downstream infinity ($X_1 \rightarrow \infty$) is in another equilibrium state with density ρ_+ , flow velocity $\mathbf{v}_+ = (v_+, 0, 0)$ ($v_+ > 0$), and temperature T_+ . We investigate the steady behavior of the gas under the following assumptions:

- (i) The specific heat at constant volume C_v is a given function $C_v(T)$ of the temperature T (thermally perfect gas).
- (ii) The behavior of the gas is described by the ES model of the Boltzmann equation proposed in Sect. 2.
- (iii) The problem is spatially one dimensional, so that the physical quantities are independent of X_2 and X_3 .

Let us denote by M_- the Mach number of the flow at upstream infinity and by γ_- the ratio of the specific heats there, i.e.,

$$M_- = \frac{v_-}{\sqrt{\gamma_- RT_-}}, \quad \gamma_- = \gamma(T_-) = \frac{C_v(T_-) + R}{C_v(T_-)}. \quad (18)$$

The downstream quantities ρ_+ , v_+ , and T_+ are related with the upstream quantities ρ_- , v_- , and T_- and the upstream Mach number M_- by the Rankine–Hugoniot relations, which take different forms depending on whether $\theta \neq 0$ or 0. To be more specific,

Proposition 6 (Rankine–Hugoniot relations for $\theta \neq 0$): When $\theta \neq 0$, the ratios ρ_+/ρ_- , v_+/v_- , and T_+/T_- are expressed in the following form:

$$\frac{\rho_+}{\rho_-} = \left(\frac{v_+}{v_-}\right)^{-1}, \quad \frac{v_+}{v_-} = \frac{1 + \gamma_- M_-^2 - \sqrt{2\gamma_- M_-^2 \hat{d}_E(\tau) + 1}}{\gamma_- M_-^2}, \quad \frac{T_+}{T_-} = \tau, \quad (19)$$

where the function $\hat{d}_E(x)$ is defined by

$$\hat{d}_E(x) = \frac{1}{R} \int_1^x C_v(T_- s) ds, \quad (20)$$

and τ is the solution, such that $\tau > 1$, of the following equation:

$$\tau + 2\hat{d}_E(\tau) + \frac{1}{\gamma_- M_-^2} - \left(\frac{1}{\sqrt{\gamma_-} M_-} + \sqrt{\gamma_-} M_- \right) \sqrt{2\hat{d}_E(\tau) + \frac{1}{\gamma_- M_-^2}} = 0. \quad (21)$$

If $C_v(T)$ is a monotonically increasing function of T , such τ is unique.

Proposition 6' (Rankine–Hugoniot relations for $\theta = 0$): For given upstream parameters ρ_- , v_- , $T_{\text{tr}-}$, and $T_{\text{int}-}$, the additional upstream parameters T_- and δ_- are determined by

$$\delta_- = D(T_-), \quad T_- = E^{-1}(3RT_{\text{tr}-}/2 + \delta_- RT_{\text{int}-}/2). \quad (22)$$

Then, the downstream parameters ρ_+ , v_+ , and $T_{\text{tr}+}$ are determined by

$$\frac{\rho_+}{\rho_-} = \frac{4\widetilde{M}_-^2}{\widetilde{M}_-^2 + 3}, \quad \frac{v_+}{v_-} = \frac{\widetilde{M}_-^2 + 3}{4\widetilde{M}_-^2}, \quad \frac{T_{\text{tr}+}}{T_{\text{tr}-}} = \frac{(5\widetilde{M}_-^2 - 1)(\widetilde{M}_-^2 + 3)}{16\widetilde{M}_-^2}, \quad (23)$$

where

$$\widetilde{M}_- = \frac{v_-}{\sqrt{5RT_{\text{tr}-}/3}} = M_- \sqrt{\frac{3\gamma_-}{5(T_{\text{tr}-}/T_-)}}. \quad (24)$$

In addition, the additional downstream parameters T_+ , $T_{\text{int}+}$, and δ_+ , where $\delta_+ = D(T_+)$, are determined by

$$\begin{aligned} \frac{E(T_+) - E(T_-)}{RT_-} &= \frac{3}{2} \left(\frac{T_{\text{tr}+}}{T_{\text{tr}-}} - 1 \right) \frac{T_{\text{tr}-}}{T_-}, & \frac{T_{\text{int}+}}{T_{\text{int}-}} &= \frac{\delta_-}{\delta_+}, \\ \delta_+ &= \frac{T_-}{T_+} \left[3 + \delta_- + 2 \frac{E(T_+) - E(T_-)}{RT_-} \right] - 3. \end{aligned} \quad (25)$$

4.2 Basic equation

The present shock-structure problem is a time-independent and spatially one-dimensional problem where f is expressed as $f = f(X_1, \boldsymbol{\xi}, \mathcal{E})$. Therefore, the basic equation is (2) with $\partial f/\partial t = \partial f/\partial X_2 = \partial f/\partial X_3 = 0$. Consistently, all the macroscopic quantities in (3)–(6) are the functions of X_1 only, and $\mathbf{v} = (v_1, 0, 0)$.

The boundary conditions at upstream and downstream infinities are expressed in the following form using the equilibrium distribution (11):

$$f = \frac{\rho_- \mathcal{E}^{\delta_-/2-1}}{(2\pi RT_-)^{3/2} (RT_-)^{\delta_-/2} \Gamma(\delta_-/2)} \exp\left(-\frac{(\xi_1 - v_-)^2 + \xi_2^2 + \xi_3^2}{2RT_-} - \frac{\mathcal{E}}{RT_-}\right), \quad (X_1 \rightarrow -\infty), \quad (26a)$$

$$f = \frac{\rho_+ \mathcal{E}^{\delta_+/2-1}}{(2\pi RT_+)^{3/2} (RT_+)^{\delta_+/2} \Gamma(\delta_+/2)} \exp\left(-\frac{(\xi_1 - v_+)^2 + \xi_2^2 + \xi_3^2}{2RT_+} - \frac{\mathcal{E}}{RT_+}\right), \quad (X_1 \rightarrow \infty), \quad (26b)$$

where we should recall that $\delta_- = D(T_-)$ and $\delta_+ = D(T_+)$.

4.3 Numerical analysis and results

We solve the system consisting of the basic equation (2) (with $\partial f/\partial t = \partial f/\partial X_2 = \partial f/\partial X_3 = 0$) and the boundary conditions (26) numerically by a finite-difference method. In this article, leaving the description of the numerical method to [4, 5], we show only the result of numerical analysis. We first mention the actual setting of the parameters and then show the computed profiles of the macroscopic quantities.

4.3.1 Parameter setting

We consider CO_2 gas and set the parameters basically following [8, 10]. We set the upstream temperature T_- and pressure p_- to be $T_- = 295$ K and $p_- = 69$ mmHg, respectively, and use the formula $C_v(T)/R = 1.412 + 8.697 \times 10^{-3}T - 6.575 \times 10^{-6}T^2 + 1.987 \times$

Table 1: Downstream states for $M_- = 1.3$ and 5. The corresponding values for constant C_v [$C_v(T) = C_v(T_-)$] are shown in the parentheses

	$M_- = 1.3$	$M_- = 5$
ρ_+/ρ_-	1.566 (1.554)	7.819 (6.199)
$v_+/(2RT_-)^{1/2}$	0.666 (0.671)	0.513 (0.648)
T_+/T_-	1.141 (1.143)	3.723 (4.522)
δ_+	3.940	5.910
$C_v(T_+)/R$	3.671	5.665
$\gamma(T_+)$	1.272	1.177

Table 2: Downstream states for $M_- = 1.3$ and 5 in the case of $\theta = 0$ (or $\mu_b/\mu = \infty$). See the caption of Table 1

	$M_- = 1.3$	$M_- = 5$
\tilde{M}_-	1.143	4.398
ρ_+/ρ_-	1.214	3.463
$v_+/(2RT_-)^{1/2}$	0.860	1.159
T_+/T_-	1.060 (1.061)	2.947 (3.564)
$T_{\text{tr}+}/T_-$	1.140	6.909
$T_{\text{int}+}/T_-$	0.999	0.730
δ_+	3.918	5.362

$10^{-9}T^3$ for $C_v(T)$ derived in [10] from the experimental data, where the coefficients have suitable dimensions in such a way that each term on the right-hand side is dimensionless. Then, we have $C_v(T_-)/R = 3.456$, $\delta_- = 2C_v(T_-)/R - 3 = 3.913$, and $\gamma_- = 1.289$. Further, the $E(T)$ can be defined consistently as $E(T) = \int_{T_-}^T C_v(s)ds + T_-C_v(T_-)$ [cf. the paragraph containing (3) in [5]]. In [8], it is assumed that $\mu \propto T^{0.935}$, so that we set $A_c(T) \propto T^{0.065}$ from (17). It should be noted, however, that although $\mu_b \propto T^{0.935}$ and $\lambda \propto T^{0.935}C_v(T)/R$ are also assumed in [8], our model cannot be made to adjust to these forms because of (17). In other words, if the parameters ν and θ have been fixed, the choice of $C_v(T)$ and $A_c(T)$ completely determines μ , μ_b , and λ according to (17) in the present model. We determine the values of ν and θ from the values of Pr and μ_b/μ at $T = T_-$ using (17). More specifically, we set Pr = 0.73 and consider some different values of μ_b/μ at $T = T_-$, i.e., $(\mu_b/\mu)_{T=T_-} = 100, 200, 500, 1000, 2000, 5200$, and ∞ . The reason why we vary $(\mu_b/\mu)_{T=T_-}$ is that though μ_b/μ is known to be very large, the

Table 3: Values of ν and θ for Pr = 0.73 and $(\mu_b/\mu)_{T=T_-} = 100, 200, 500, 1000, 2000, 5200$, and ∞

$(\mu_b/\mu)_{T=T_-}$	100	200	500	1000	2000	5200	∞
$-\nu \times 10$	3.718	3.708	3.702	3.701	3.700	3.699	3.699
$\theta \times 10^4$	51.69	25.85	10.34	5.169	2.585	0.9941	0

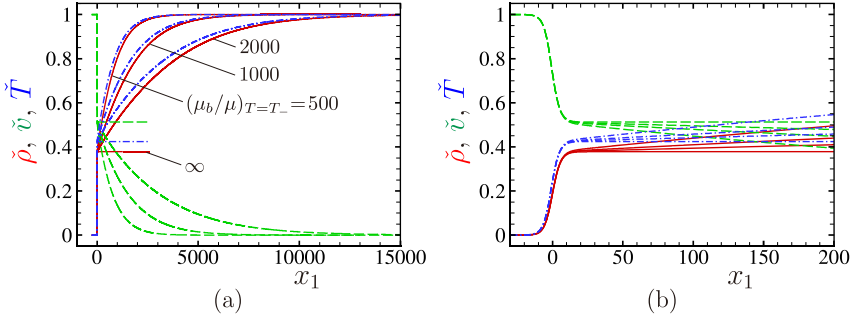


Fig. 1: Profiles of $\check{\rho}$, \check{v} , and \check{T} at $M_- = 1.3$ for $(\mu_b/\mu)_{T=T_-} = 500, 1000, 2000,$ and ∞ . (a) Profiles for $-1000 \leq x_1 \leq 15000$, (b) profiles for $-30 \leq x_1 \leq 200$. The solid line indicates $\check{\rho}$, the dashed line \check{v} , and the dot-dashed line \check{T} .

value is not known precisely and that we are interested in the behavior of a polyatomic gas when μ_b/μ becomes large. Therefore, as in [4], we consider a *pseudo*-CO₂ gas with variable $(\mu_b/\mu)_{T=T_-}$.

In [4], we showed the profiles of macroscopic quantities across a shock wave of Types A, B, and C, where these types are defined in [8]. That is, Type A indicates a smooth and symmetric profile that is realized when M_- is close to 1; Type C is a profile with a double-layer structure composed of a thin front layer with rapid change and a thick rear layer with slow relaxation of the internal modes that appears when M_- is slightly larger; and Type B indicates a non-symmetric profile with a corner upstream that occurs at the transition from Type A to Type C. The ES model with constant specific heats, which was used in [4], is legitimated for Type-A and B profiles because the temperature rise across the shock wave is small in these cases. Therefore, in the present study, we concentrate on the Type-C profile. Since the transition from Type A to Type C takes place at $M_- = 1.137$ in the present parameter setting, we carry out the computation for $M_- = 1.3, 1.47, 3,$ and 5 following [8, 10]. However, to save space, we will present the results only for $M_- = 1.3$ and 5 . The downstream states for $M_- = 1.3$ and 5 are shown in Table 1, and the corresponding values for $\theta = 0$ (or $\mu_b/\mu = \infty$), including the values of \widetilde{M}_- that is defined in Proposition 6' [i.e., (24) with $T_{\text{tr}} = T_-$], are shown in Table 2. The values of ν and θ corresponding to our choices of Pr and $(\mu_b/\mu)_{T=T_-}$ are shown in Table 3.

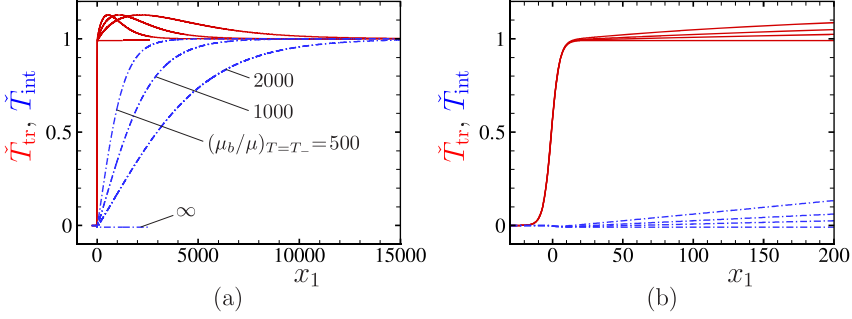


Fig. 2: Profiles of \check{T}_{tr} and \check{T}_{int} at $M_- = 1.3$ for $(\mu_b/\mu)_{T=T_-} = 500, 1000, 2000,$ and ∞ . (a) Profiles for $-1000 \leq x_1 \leq 15000$, (b) profiles for $-30 \leq x_1 \leq 200$. The solid line indicates \check{T}_{tr} and the dot-dashed line \check{T}_{int} .

4.3.2 Profiles of macroscopic quantities

We show the profiles of the density ρ , the flow velocity v_1 (the X_1 component), and the temperatures T , T_{tr} , and T_{int} normalized in the conventional way, i.e.,

$$\begin{aligned} \check{\rho} &= \frac{\rho - \rho_-}{\rho_+ - \rho_-}, & \check{v} &= \frac{v_1 - v_+}{v_- - v_+}, & \check{T} &= \frac{T - T_-}{T_+ - T_-}, \\ \check{T}_{\text{tr}} &= \frac{T_{\text{tr}} - T_-}{T_+ - T_-}, & \check{T}_{\text{int}} &= \frac{T_{\text{int}} - T_-}{T_+ - T_-}. \end{aligned} \quad (27)$$

In this normalization, $\check{\rho}$, \check{T} , \check{T}_{tr} , and \check{T}_{int} varies from 0 (upstream infinity) to 1 (downstream infinity), whereas \check{v} from 1 (upstream infinity) to 0 (downstream infinity). In addition, we only show the results for large values of $(\mu_b/\mu)_{T=T_-}$, i.e., $(\mu_b/\mu)_{T=T_-} = 500, 1000, 2000,$ and ∞ . To show the profiles in Fig. 1–5 below, we use the dimensionless coordinate x_1 scaled with the mean free path l_- of the gas molecules in the equilibrium state at rest at density ρ_- and temperature T_- , that is,

$$x_1 = \frac{X_1}{l_-}, \quad l_- = \frac{2}{\sqrt{\pi}} \frac{(2RT_-)^{1/2}}{A_c(T_-)\rho_-}. \quad (28)$$

In Fig. 1, we show the profiles of $\check{\rho}$, \check{v} , and \check{T} at $M_- = 1.3$ for $(\mu_b/\mu)_{T=T_-} = 500, 1000, 2000,$ and ∞ . Figure 1(b) is the magnified figure of Fig. 1(a) in the range $-30 \leq x_1 (= X_1/l_-) \leq 200$. The solid line indicates $\check{\rho}$, the dashed line \check{v} , and the dot-dashed line \check{T} . Note that for $(\mu_b/\mu)_{T=T_-} = \infty$, the downstream condition is different from that for finite $(\mu_b/\mu)_{T=T_-}$ and is given by the Rankine–Hugoniot relations for $(\mu_b/\mu)_{T=T_-} = \infty$ or $\theta = 0$ [(23)–(25); note that $T_{\text{tr}-} = T_{\text{int}-} = T_-$ in the present problem]. In this figure and the following Figs. 2–5, $x_1 = 0$ is set at the position where the density is equal to the average of the upstream and downstream values when $(\mu_b/\mu)_{T=T_-} = \infty$. The profiles, which are of Type C, consist of a thin front layer and a thick rear layer. As $(\mu_b/\mu)_{T=T_-}$

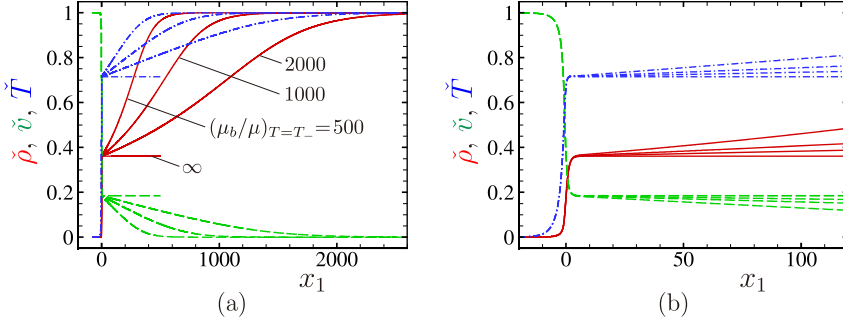


Fig. 3: Profiles of $\check{\rho}$, \check{v} , and \check{T} at $M_- = 5$ for $(\mu_b/\mu)_{T=T_-} = 500, 1000, 2000$, and ∞ . (a) Profiles for $-200 \leq x_1 \leq 2600$, (b) profiles for $-20 \leq x_1 \leq 120$. See the caption of Fig. 1.

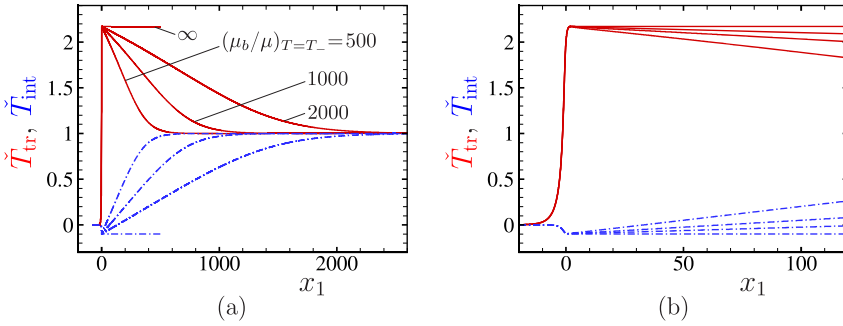


Fig. 4: Profiles of \check{T}_{tr} and \check{T}_{int} at $M_- = 5$ for $(\mu_b/\mu)_{T=T_-} = 500, 1000, 2000$, and ∞ . (a) Profiles for $-200 \leq x_1 \leq 2600$, (b) profiles for $-20 \leq x_1 \leq 120$. See the caption of Fig. 2.

increases, the thickness of the rear layer increases and reaches over 15000 mean free paths (l_-) for $(\mu_b/\mu)_{T=T_-} = 2000$, whereas the profiles of the thin front layer are not affected by $(\mu_b/\mu)_{T=T_-}$ and coincide with the shock profiles for $(\mu_b/\mu)_{T=T_-} = \infty$.

Figure 2 shows the profiles of \check{T}_{tr} and \check{T}_{int} in the same case as Fig. 1. Figure 2(b) is the magnified figure of Fig. 2(a) in the range $-30 \leq x_1 \leq 200$. The solid line indicates \check{T}_{tr} and the dot-dashed line \check{T}_{int} . A significant overshoot is observed for \check{T}_{tr} .

Next, we show the profiles at a higher Mach number, $M_- = 5$, for $(\mu_b/\mu)_{T=T_-} = 500, 1000, 2000$, and ∞ . Figure 3 shows the profiles of $\check{\rho}$, \check{v} , and \check{T} , and Fig. 4 those of \check{T}_{tr} and \check{T}_{int} . Figures 3(b) and 4(b) are, respectively, the magnified figures of Figs. 3(a) and 4(a) in the range $-20 \leq x_1 (= X_1/l_-) \leq 120$, and the types of lines are the same as Figs. 1 and 2, i.e., the solid line indicates $\check{\rho}$, the dashed line \check{v} , and the dot-dashed line \check{T} in Fig. 3; the solid line indicates \check{T}_{tr} , and the dot-dashed line \check{T}_{int} in Fig. 4.

In this case ($M_- = 5$), the shock wave is thinner than that at $M_- = 1.3$ for the same $(\mu_b/\mu)_{T=T_-}$ and extend over 2600 mean free paths when $(\mu_b/\mu)_{T=T_-} = 2000$. The change of the profiles over the thin front layer at $M_- = 5$ is steeper than that at $M_- = 1.3$. As

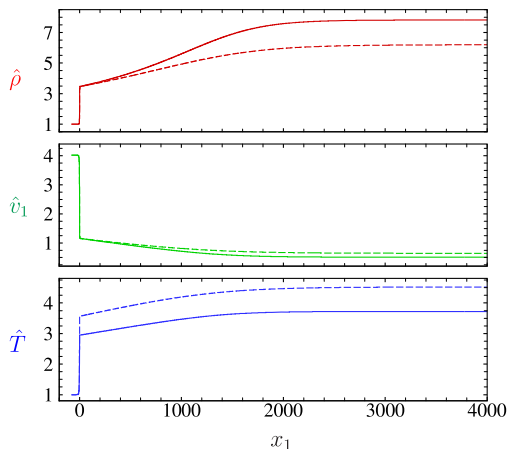


Fig. 5: Comparison of the profiles of $\hat{\rho}$ ($= \rho/\rho_-$), \hat{v}_1 [$= v_1/(2RT_-)^{1/2}$], and \hat{T} ($= T/T_-$) at $M_- = 5$ for $(\mu_b/\mu)_{T=T_-} = 2000$. The solid line indicates the case of temperature-dependent specific heats (or temperature-dependent δ) and the dashed line the case of constant specific heats [or constant δ ($= \delta_-$)].

one can see from Table 1, the values of the macroscopic quantities at downstream infinity are very different from those for a gas with constant specific heats, so that the profiles over the thick layer are significantly affected by the temperature-dependent specific heats. The profiles of the dimensionless density $\hat{\rho}$, flow velocity \hat{v}_1 , and temperature \hat{T} , where

$$\hat{\rho} = \rho/\rho_-, \quad \hat{v}_1 = v_1/(2RT_-)^{1/2}, \quad \hat{T} = T/T_-, \quad (29)$$

are compared between the case of temperature-dependent specific heats (or temperature-dependent δ) and the case of constant specific heats [or constant δ ($= \delta_-$)] in Fig. 5 for $M_- = 5$ and $(\mu_b/\mu)_{T=T_-} = 2000$.

Finally, we should mention that we have also compared our numerical results with the results based on the extended thermodynamics in [10] and obtained very good agreement.

4.4 Slowly varying solution

In [4], a set of macroscopic equations that describes slow relaxation of the internal modes over the thick rear layer in Type-C solution (and the entire profiles of Type-A and B solutions) when the ratio μ_b/μ is large (i.e., θ is small) has been obtained by considering a slowly varying solution whose length scale of variation in X_1 is l_-/θ . This system is convenient because one can obtain an analytical solution of the shock profiles. In fact, the corresponding system for the present new ES model has been derived in Appendix C in [5] and analyzed in Sect. 3.7. Here, we will omit the derivation and show only the analysis of the system.

If we introduce appropriate dimensionless variables, the basic equation (2) with $\partial f/\partial t = \partial f/\partial X_2 = \partial f/\partial X_3 = 0$ is transformed into the following dimensionless form:

$$\zeta_1 \frac{\partial \hat{f}}{\partial x_1} = \frac{2}{\sqrt{\pi}} \hat{A}_c(\hat{T}) \hat{\rho} (\hat{\mathcal{G}} - \hat{f}), \quad (30)$$

where x_1 is defined by (28), $\hat{\rho}$ and \hat{T} are defined by (29), and

$$\zeta_i = \xi_i/(2RT_-)^{1/2}, \quad (\hat{f}, \hat{\mathcal{G}}) = (f, \mathcal{G})(2RT_-)^{5/2}/2\rho_-, \quad \hat{A}_c(\hat{T}) = A_c(T)/A_c(T_-). \quad (31)$$

See Sect. 3.2 in [5] for the explicit form of $\hat{\mathcal{G}}$. In the following, we also need the dimensionless counterpart of v_1 , T_{tr} , T_{int} , and $E(T)$, that is, \hat{v}_1 defined by (29), and \hat{T}_{tr} , \hat{T}_{int} , and $\hat{E}(\hat{T})$ defined by

$$\hat{T}_{\text{tr}} = T_{\text{tr}}/T_-, \quad \hat{T}_{\text{int}} = T_{\text{int}}/T_-, \quad \hat{E}(\hat{T}) = E(T)/RT_-. \quad (32)$$

We consider the solution of (30) whose length scale of variation in x_1 is $1/\theta$. Therefore, we introduce the new space coordinate y_1 defined by

$$y_1 = (2/\sqrt{\pi})\theta x_1. \quad (33)$$

Then, (30) becomes

$$\zeta_1 \frac{\partial \hat{f}}{\partial y_1} = \frac{1}{\theta} \hat{A}_c(\hat{T}) \hat{\rho} (\hat{\mathcal{G}} - \hat{f}). \quad (34)$$

We seek the solution in the form of expansion in the small parameter θ :

$$\hat{f} = \hat{f}^{(0)} + \hat{f}^{(1)}\theta + \hat{f}^{(2)}\theta^2 + \dots. \quad (35)$$

Correspondingly, the macroscopic quantities $\hat{\rho}$, \hat{v}_1 , \hat{T}_{tr} , \hat{T}_{int} , etc. are expanded as

$$h = h^{(0)} + h^{(1)}\theta + h^{(2)}\theta^2 + \dots, \quad (36)$$

where h stands for $\hat{\rho}$, \hat{v}_1 , \hat{T}_{tr} , \hat{T}_{int} , etc. This is basically the same as the procedure of the Hilbert expansion, and we can derive the ordinary differential equations for the macroscopic quantities $\hat{\rho}^{(m)}$, $\hat{v}_1^{(m)}$, $\hat{T}_{\text{tr}}^{(m)}$, and $\hat{T}_{\text{int}}^{(m)}$. In [5], we have derived the equations only at the zeroth order, i.e., those for $\hat{\rho}^{(0)}$, $\hat{v}_1^{(0)}$, $\hat{T}_{\text{tr}}^{(0)}$, and $\hat{T}_{\text{int}}^{(0)}$ (see Appendix C in [5] for the detailed derivation).

If we omit the superscript (0) to avoid cumbersome notation, the resulting equations for the zeroth-order quantities are expressed as follows:

$$\frac{d}{dy_1} (\hat{\rho} \hat{v}_1) = 0, \quad (37a)$$

$$\frac{d}{dy_1} \left(\frac{\hat{T}_{\text{tr}}}{\hat{v}_1} + 2\hat{v}_1 \right) = 0, \quad (37b)$$

$$\frac{d}{dy_1} \left(\hat{v}_1^2 + \frac{5}{2}\hat{T}_{\text{tr}} + \frac{\delta}{2}\hat{T}_{\text{int}} \right) = 0, \quad (37c)$$

$$\hat{v}_1 \frac{d}{dy_1} (\delta \hat{T}_{\text{int}}) = \frac{3\delta}{3+\delta} \hat{A}_c(\hat{T}) \hat{\rho} (\hat{T}_{\text{tr}} - \hat{T}_{\text{int}}), \quad (37d)$$

where

$$\delta = \hat{D}(\hat{T}) = \frac{2}{\hat{T}} \hat{E}(\hat{T}) - 3, \quad \hat{T} = \hat{E}^{-1}(3\hat{T}_{\text{tr}}/2 + \delta\hat{T}_{\text{int}}/2), \quad (38)$$

so that the relation

$$\hat{T} = \frac{3\hat{T}_{\text{tr}} + \delta\hat{T}_{\text{int}}}{3 + \delta}, \quad (39)$$

holds. Here, we have used (37a) in deriving (37b) and (37c) and used (39) in deriving (37d). Hereafter, we consider (37) supplemented by the first equation of (38) and (39) as the closed system to be solved. It should be noted that (37) is the steady version of a hyperbolic conservation system with relaxation, a simplified model of which has been studied in mathematical rigor [6].

As in Sect. V A in [4], it follows from (37a)–(37c) that [cf. (57) in [4]]

$$\hat{\rho} = \frac{c_1}{\hat{v}_1}, \quad \hat{T}_{\text{tr}} = \hat{v}_1 (c_2 - 2\hat{v}_1), \quad \hat{T}_{\text{int}} = \frac{2}{\delta} \left(c_3 - \frac{5}{2}c_2\hat{v}_1 + 4\hat{v}_1^2 \right), \quad (40)$$

where c_1 , c_2 , and c_3 are constants. Inserting (40) in (37d) and (39), we obtain the following equations [cf. (58) in [4]]:

$$\hat{v}_1^2 \left(\frac{5}{16}c_2 - \hat{v}_1 \right) \frac{d\hat{v}_1}{dy_1} = \frac{3}{8(3 + \delta)} c_1 \hat{A}_c(\hat{T}) \left[(4 + \delta)\hat{v}_1^2 - \frac{5 + \delta}{2}c_2\hat{v}_1 + c_3 \right], \quad (41a)$$

$$\delta = \hat{D}(\hat{T}), \quad \hat{T} = \frac{2}{3 + \delta} (\hat{v}_1^2 - c_2\hat{v}_1 + c_3). \quad (41b)$$

Since δ and \hat{T} can be, in principle, expressed in terms of \hat{v}_1 from (41b), (41a) is the equation for \hat{v}_1 . If we eliminate c_3 from (41a) using (41b), we have an alternative expression of (41a), i.e.,

$$\hat{v}_1^2 \left(\frac{5}{16}c_2 - \hat{v}_1 \right) \frac{d\hat{v}_1}{dy_1} = \frac{3}{8} c_1 \hat{A}_c(\hat{T}) \left(\hat{v}_1^2 - \frac{1}{2}c_2\hat{v}_1 + \frac{1}{2}\hat{T} \right). \quad (42)$$

As discussed in [4], the slowly varying solution describes either the full shock profiles (Type-A and Type-B profiles) or the profiles of the thick rear layer (Type-C profile). Therefore, $(\hat{\rho}, \hat{v}_1, \hat{T}_{\text{tr}}, \hat{T}_{\text{int}})$ should approach $(\hat{\rho}_+, \hat{v}_+, \hat{T}_+, \hat{T}_+)$ as $x_1 \rightarrow \infty$, where $(\hat{\rho}_+, \hat{v}_+, \hat{T}_+) = (\rho_+/\rho_-, v_+/(2RT_-)^{1/2}, T_+/T_-)$. If we consider this limit in (40), we have

$$c_1 = \hat{\rho}_+\hat{v}_+, \quad c_2 = (\hat{T}_+/\hat{v}_+) + 2\hat{v}_+, \quad c_3 = \hat{v}_+^2 + [(5 + \delta_+)/2]\hat{T}_+. \quad (43)$$

However, the conservations of mass, momentum, and energy between the upstream and downstream infinities and the fact that $\hat{E}(1) = (3 + \delta_-)/2$ and $\hat{E}(\hat{T}_+) = [(3 + \delta_+)/2]\hat{T}_+$ show that the right-hand sides of three equations of (43) are equal to \hat{v}_- , $(1/\hat{v}_-) + 2\hat{v}_-$,

and $\hat{v}_-^2 + (5 + \delta_-)/2$, respectively, where $\hat{v}_- = v_-/(2RT_-)^{1/2}$. Therefore, c_1 , c_2 , and c_3 are expressed, in terms of the upstream quantities, as

$$c_1 = \hat{v}_-, \quad c_2 = \frac{1}{\hat{v}_-} + 2\hat{v}_-, \quad c_3 = \hat{v}_-^2 + \frac{5 + \delta_-}{2}. \quad (44)$$

By using (44), we can transform (42) and (41b) into the following form:

$$\hat{v}_1^2(\hat{v}_* - \hat{v}_1) \frac{d\hat{v}_1}{dy_1} = \frac{3\hat{v}_-}{8} \hat{A}_c(\hat{T}) \left(\hat{v}_1^2 - \frac{1 + 2\hat{v}_-^2}{2\hat{v}_-} \hat{v}_1 + \frac{1}{2} \hat{T} \right), \quad (45a)$$

$$\delta = \hat{D}(\hat{T}), \quad (45b)$$

$$\hat{T} = \frac{2}{3 + \delta} \left[\frac{3 + \delta_-}{2} + (\hat{v}_1 - \hat{v}_-) \left(\hat{v}_1 - \frac{1 + \hat{v}_-^2}{\hat{v}_-} \right) \right], \quad (45c)$$

where

$$\hat{v}_* = \frac{5}{16} \frac{1 + 2\hat{v}_-^2}{\hat{v}_-}, \quad (46)$$

and we should recall that $\delta_- = \hat{D}(1)$. When $\hat{v}_1 = \hat{v}_-$, (38) and (45c) show that $\hat{E}(\hat{T}) = [(3 + \delta)/2]\hat{T} = (3 + \delta_-)/2 = \hat{E}(1)$, so that $\hat{T} = 1$ and thus $\delta = \delta_-$. In this case, it is readily seen that the right-hand side of (45a) vanishes. Therefore, $\hat{v}_1 = \hat{v}_-$ is an equilibrium point of (45a) if $\hat{v}_* \neq \hat{v}_-$. On the other hand, if we use (43) in (41), we obtain (45a) and (45c) with alternative expressions of the right-hand sides in terms of the downstream quantities δ_+ [= $\hat{D}(\hat{T}_+)$], \hat{v}_+ , and \hat{T}_+ [and $\hat{\rho}_+$ for (45a)]. From these expressions, we can readily see that when $\hat{v}_1 = \hat{v}_+$, it follows that $\hat{T} = \hat{T}_+$ and thus $\delta = \delta_+$. Therefore, it is easy to see that the right-hand side of (45a) vanishes at $\hat{v}_1 = \hat{v}_+$, that is, it is an equilibrium point of (45a) if $\hat{v}_* \neq \hat{v}_+$. The (local) stability of the equilibrium points is discussed in Appendix D in [5].

Once \hat{v}_1 is obtained from (45), other quantities follow from (40) with (44), i.e.,

$$\hat{\rho}(\hat{v}_1) = \frac{\hat{v}_-}{\hat{v}_1}, \quad \hat{T}_{\text{tr}}(\hat{v}_1) = 1 + 2(\hat{v}_- - \hat{v}_1) \left(\hat{v}_1 - \frac{1}{2\hat{v}_-} \right), \quad (47a)$$

$$\hat{T}_{\text{int}}(\hat{v}_1) = \frac{\delta_-}{\delta} + \frac{8}{\delta} (\hat{v}_1 - \hat{v}_-) (\hat{v}_1 - \hat{v}_{**}), \quad (47b)$$

where

$$\hat{v}_{**} = \frac{5 + 2\hat{v}_-^2}{8\hat{v}_-}, \quad (48)$$

which is the dimensionless downstream velocity of the shock wave when $\theta = 0$ corresponding to v_+ in (23). When $\hat{v}_1 = \hat{v}_-$, we have $\hat{\rho} = \hat{T}_{\text{tr}} = \hat{T}_{\text{int}} = 1$ because $\delta = \delta_-$. Similarly, from the alternative expressions of $\hat{\rho}$, \hat{T}_{tr} , and \hat{T}_{int} obtained by using (43) in (40), it is seen that when $\hat{v}_1 = \hat{v}_+$, we have $\hat{\rho} = \hat{\rho}_+$ and $\hat{T}_{\text{tr}} = \hat{T}_{\text{int}} = \hat{T}_+$.

Since (45) is more implicit than the corresponding equation, (60) in [4], in the case of constant δ , we can obtain less information about the global behavior of the solution. However, according to the stability analysis in Appendix D in [5], we can expect the basic properties of (60) in [4] are retained in (45). Therefore, we try to integrate it in the similar way as in [4]. From (45a), we obtain

$$\frac{dy_1}{d\hat{v}_1} = \frac{8}{3\hat{v}_-} \frac{\hat{v}_1^2(\hat{v}_* - \hat{v}_1)}{\hat{A}_c(\hat{T}) \left(\hat{v}_1^2 - \frac{1 + 2\hat{v}_-^2}{2\hat{v}_-} \hat{v}_1 + \frac{1}{2} \hat{T} \right)}. \quad (49)$$

Assuming that \hat{v}_1 is a decreasing function of y_1 , which is likely to be true from the numerical results, we integrate (49) from \hat{v}_1 to \hat{v}_0 to obtain

$$y_1(\hat{v}_1) - y_0 = -\frac{8}{3\hat{v}_-} \int_{\hat{v}_1}^{\hat{v}_0} \frac{u^2(\hat{v}_* - u)}{\hat{A}_c(\hat{T}) \left(u^2 - \frac{1 + 2\hat{v}_-^2}{2\hat{v}_-} u + \frac{1}{2} \hat{T} \right)} du, \quad (50)$$

where

$$\delta = \hat{D}(\hat{T}), \quad (51a)$$

$$\hat{T} = \frac{2}{3 + \delta} \left[\frac{3 + \delta_-}{2} + (u - \hat{v}_-) \left(u - \frac{1 + \hat{v}_-^2}{\hat{v}_-} \right) \right], \quad (51b)$$

and $y_0 = y_1(\hat{v}_0)$. The inverse function of $y_1(\hat{v}_1)$ gives the velocity profile $\hat{v}_1(y_1)$ with the initial condition $\hat{v}_1 = \hat{v}_0$ at $y_1 = y_0$.

As in [4], we can make the following settings of y_0 and \hat{v}_0 depending on the upstream Mach number M_- as well as the effective upstream Mach number \widetilde{M}_- for $\theta = 0$ that is defined by (24) (note that $T_{tr-} = T_-$ in the present problem; see also Appendix D in [5]):

(i) For $\widetilde{M}_- < 1 < M_-$, we let $y_0 = -\infty$ and $\hat{v}_0 = \hat{v}_-$. Then, the resulting profiles of $\hat{v}_1(y_1)$ and other macroscopic quantities exhibit the entire profiles of Type A.

(ii) For $1 < \widetilde{M}_- (< M_-)$, we let $y_0 = 0$ and $\hat{v}_0 = \hat{v}_{**}$ defined by (48). Then, the resulting profiles of $\hat{v}_1(y_1)$ and other macroscopic quantities demonstrate the profiles in the thick rear layer of Type-C solution.

(iii) For $\widetilde{M}_- = 1 (< M_-)$, we let $y_0 = 0$ and $\hat{v}_0 = \hat{v}_-$. Then, the profiles of $\hat{v}_1(y_1)$ and other macroscopic quantities show the entire profiles of Type B with a corner at the start of the profiles $y_1 = 0$.

Now we compare the solution (50) in case (ii) (Type-C profile) with the numerical results that were shown in Figs. 1, 2, 3, and 4. Figures 6(a) and 6(b) are, respectively, the same as Figs. 1(a) and 2(a) for $M_- = 1.3$, but y_1 is used instead of x_1 . Therefore, the curves for $(\mu_b/\mu)_{T=T_-} = 500, 1000, \text{ and } 2000$ coincide except in the thin front layer. The result obtained from (50) is shown by the cross symbol at discrete points of y_1 to make the comparison clear. Figures 7(a) and 7(b) are, respectively, the same as Figs. 3(a) and

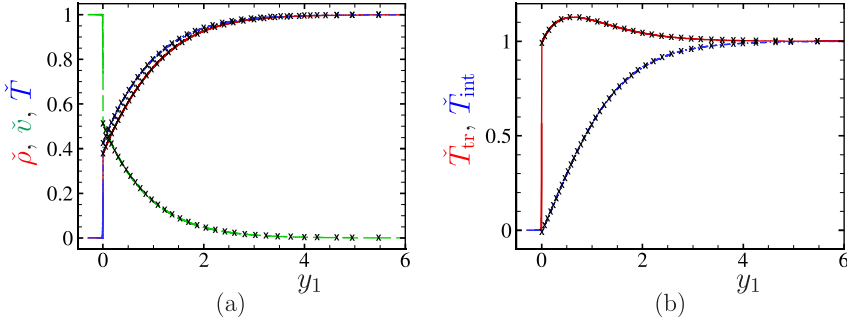


Fig. 6: Comparison between the profiles based on the slowly varying solution and those based on the numerical solution at $M_- = 1.3$. (a) Profiles of $\tilde{\rho}$, \tilde{v} , and \tilde{T} , (b) profiles of \tilde{T}_{tr} and \tilde{T}_{int} . The cross symbol indicates the slowly varying solution, and the curves indicate the numerical solution for $(\mu_b/\mu)_{T=T_-} = 500, 1000, \text{ and } 2000$. See Figs. 1(a) and 2(a) and the captions of Figs. 1 and 2.

4(a) for $M_- = 5$, and the manner of comparison is the same as in Fig. 6. The figures show perfect agreement between the solution based on (50) and numerical solution using the new ES model.

As remarked at the end of Appendix C.2 in [5], the macroscopic equations used here are essentially the same as the ET6 system that has been used to analyze the shock-wave structure in [9, 10, 7]. In these references, to describe the Type-C profile, the weak solution of the ET6 system has been considered, that is, a sub-shock with an appropriate jump condition is set and is connected with the solution of ET6 system. In the present section, as well as Sect. V in [4], we identified the thin front layer of the Type-C profile as the shock wave for $\theta = 0$ (or infinitely large μ_b/μ) numerically and combined (37) with the corresponding Rankine–Hugoniot relations to describe the Type-C profile. Since (37) is derived under the slowly varying assumption, the weak solution, which allows discontinuities, should be excluded. However, if we admit (37) as the basic equation, we can proceed in the same way as in the case of the ET6 system. It should also be mentioned that shock-wave structure for CO_2 gas was studied recently by using different continuum models, including the Navier–Stokes equations [1].

5 Concluding remarks

In the present study, we have proposed a new kinetic model for the Boltzmann equation for a polyatomic gas with temperature-dependent specific heats (thermally perfect gas) (Sect. 2). It is a straightforward extension of the conventional ES model for a gas with constant specific heats (calorically perfect gas) [2, 3]. Then, the basic properties of the new model, such as the equilibrium solution, the conservation laws, the H theorem (only in the space-homogeneous case), and the formulas of the viscosity, bulk viscosity, and

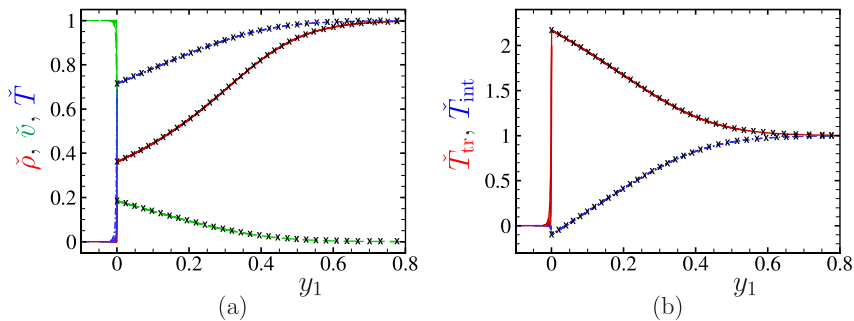


Fig. 7: Comparison between the profiles based on the slowly varying solution and those based on the numerical solution at $M_- = 5$. (a) Profiles of $\tilde{\rho}$, \tilde{v} , and \tilde{T} , (b) profiles of \tilde{T}_{tr} and \tilde{T}_{int} . See the caption of Fig. 6.

thermal conductivity, have been established (Sect. 3).

Next, the model was applied to the problem of the shock-wave structure of CO_2 gas, which is known to have a very large value of the ratio of the bulk viscosity to the viscosity (Sect. 4). First, the problem was tackled by a direct numerical analysis (Sect. 4.3), which was carried out in parallel to the case of a gas with constant specific heats [4]. The detailed profiles of macroscopic quantities across the shock wave have been shown for two typical upstream Mach numbers ($M_- = 1.3$ and 5) that provide the Type-C profile defined in [8] (i.e., the profile consisting of a thin front layer with rapid change and a thick rear layer with slow relaxation) (Sect. 4.3.2). In the case of the higher Mach number ($M_- = 5$), the effect of the temperature dependence of the specific heats has a large effect, and the profiles are significantly different from those for the gas with constant specific heats.

Following the analysis in [4], we also derived a system of macroscopic equations for the slowly varying solution that describes the slow relaxation of the internal modes. The system is an extension of the system derived in [4] to the case of temperature-dependent specific heats. The numerical computation based on the analytical solution of this system, combined with the Rankine–Hugoniot relations for infinitely large bulk viscosity, gives the profiles of the thick rear layer of Type-C profile in perfect agreement with the numerical solution of the new ES model (Sect. 4.4).

The present article is just a summary of the paper [5]. The reader who is interested in the subject is referred to the original paper [5] for the details.

References

- [1] I. V. Alekseev, A. A. Kosareva, E. V. Kustova, and E. A. Nagnibeda, Various continuum approaches for studying shock wave structure in carbon dioxide, AIP Conference Proceedings, The 8th Polyakhov’s Reading, vol. 1959, 060001. AIP, Melville (2018).

- [2] P. Andries, P. Le Tallec, J.-P. Perlat, and B. Perthame, The Gaussian-BGK model of Boltzmann equation with small Prandtl number, *Eur. J. Mech. B/Fluids*, **19**, 813–830 (2000).
- [3] S. Brull and J. Schneider, On the ellipsoidal statistical model for polyatomic gases, *Continuum Mech. Thermodyn.* **20**, 489–508 (2009).
- [4] S. Kosuge and K. Aoki, Shock-wave structure for a polyatomic gas with large bulk viscosity, *Phys. Rev. Fluids* **3**, 023401 (2018).
- [5] S. Kosuge, H.-W. Kuo, and K. Aoki, A kinetic model for a polyatomic gas with temperature-dependent specific heats and its application to shock-wave structure, *J. Stat. Phys.* **177**, 209–251 (2019).
- [6] T.-P. Liu, Hyperbolic conservation laws with relaxation, *Commun. Math. Phys.* **108**, 153–175 (1987).
- [7] M. Pavić-Čolić, D. Madjarević, and S. Simić, Polyatomic gases with dynamic pressure: Kinetic non-linear closure and the shock structure, *Int. J. Non-Linear Mech.* **92**, 160–175 (2017).
- [8] S. Taniguchi, T. Arima, T. Ruggeri, M. Sugiyama, Thermodynamic theory of the shock wave structure in a rarefied polyatomic gas: Beyond the Bethe-Teller theory, *Phys. Rev. E* **89**, 013025 (2014).
- [9] S. Taniguchi, T. Arima, T. Ruggeri, and M. Sugiyama, Effect of the dynamic pressure on the shock wave structure in a rarefied polyatomic gas, *Phys. Fluids* **26**, 016103 (2014).
- [10] S. Taniguchi, T. Arima, T. Ruggeri, M. Sugiyama, Overshoot of the non-equilibrium temperature in the shock wave structure of a rarefied polyatomic gas subject to the dynamic pressure, *Int. J. Non-Linear Mech.* **79**, 66–75 (2016).